

Dipolar Fluence distribution of statistically isotropic FERMI Gamma-Ray Bursts

Maria Lopes¹, Armando Bernui¹, Wiliam S. Hipólito-Ricaldi^{2,3}, Camila Franco¹, and Felipe Avila¹

¹Observatório Nacional, Rua General José Cristino 77, São Cristóvão, 20921-400 Rio de Janeiro, RJ, Brasil, e-mail: marialopes@on.br, bernui@on.br, camilafranco@on.br, fsavila2@gmail.com

²Departamento de Ciências Naturais, CEUNES, Universidade Federal do Espírito Santo, Rodovia BR 101 Norte, km. 60, CEP 29.932-540, São Mateus, ES, Brasil, e-mail: wiliam.ricaldi@ufes.br

³Núcleo Cosmo-UFES, Universidade Federal do Espírito Santo, Av. Fernando Ferrari, 540, CEP 29.075-910, Vitória, ES, Brasil

Abstract

We investigate the large-angle distribution of the gamma-ray bursts (GRB) from the updated FERMI/GBM catalogue, to probe the statistical isotropy of these astrophysical transient events. We also study the angular distribution of the GRB fluence, as a way to explore if this radiative feature shows some preferred direction on the sky that can suggest their origin. Our model-independent approach performs a directional analysis of the updated FERMI/GBM catalogue. The statistical significance of our results is obtained by comparison with a large set of statistically isotropic samples of cosmic objects, with the same features of the FERMI data. Our analyses confirm that the angular distribution of the FERMIGRB is statistically isotropic on the celestial sphere. Moreover, analysing the directional distribution of the FERMIGRB fluence, that is, the median GRB fluence in a set of directions that scans the celestial sphere, we found that this astrophysical property exhibits a net dipolar structure with a directional preference for latitudes near the galactic plane. However, additional studies show that this directional preference, indeed, is not correlated with the Milky Way galactic plane, suggesting that the GRB, and its fluence dipolar structure, are extra-galactic in origin. Interestingly, the analyses of the BATSE Channel 4 fluence data, that is, those GRB from BATSE with energy > 300 keV, reveal that its dipole direction is very well aligned with the cosmic microwave background dipole.

Keywords: Cosmology: observations – large-scale structure of Universe – Gamma rays: galaxies – Methods: statistical

1 Introduction

The hypothesis of statistical isotropy (SI)¹ is part of the cosmological principle (CP), a criterion that supports the concordance cosmological model Λ CDM. The study of the SI with diverse cosmic probes and different methodologies is important not only because it leads to verify the universality of the CP, but also it can provide us with new insights into the astrophysical properties of the universe (see, e.g., Colin et al.

[2011], Javanmardi et al. [2015], Tiwari and Jain [2019], Aluri et al. [2023]). For example, analyses of the cosmic microwave background data suggest isotropy violation (see, e.g., de Oliveira-Costa et al. [2004], Eriksen et al. [2004], Akrami et al. [2020], Kester et al. [2024]). These results motivated the search for a possible cause, studies that include, for instance, non-trivial topology of the universe, primordial magnetic fields, and non-standard inflation (see, e.g., Hipólito-Ricaldi and Gomero [2005], Inoue and Silk [2006], Pereira

¹We will use the term *isotropy* to refer to statistical isotropy.

et al. [2007], Bernui and Hipolito-Ricaldi [2008]). On the other hand, isotropy violation could be related to systematics, a possibility that also deserves detailed analyses [Bernui et al., 2008]. Thus, isotropy studies of cosmological tracers observed by new astronomical surveys or simply re-analyses of updated catalogs are essential to validate the CP.

The study of the angular distribution of the Gamma-ray bursts (GRB) started in the 1990's with the Burst and Transient Source Experiment (BATSE) [Fishman et al., 1994], performed with an all sky monitor 20 – 1000 keV, one of the four instruments on board the Compton Gamma-Ray Observatory (CGRO) satellite [Gehrels et al., 1993, Preece et al., 2000]. GRB are astrophysical phenomena associated to stellar catastrophic events occurring in host galaxies. Until recently, the astronomical community believed that the burst duration, T_{90} ², was the only parameter to divide the set of observed GRB into two disjoint classes [Kouveliotou et al., 1993], thus determining the astrophysical source that originates the burst by the class to which it belongs. At first, the GRB sample was divided into the short-time events, $T_{90} < 2$ s, or Short-GRB, and the long-time events, $T_{90} > 2$ s, or Long-GRB [Kouveliotou et al., 1993, Hakkila et al., 2000]. However, in recent years more information from these intriguing events has been collected, new studies on their radiative processes have been reported and, consequently, other physical features were recognised to complement the parameter T_{90} to elucidate the astrophysical source originating GRB [Hakkila et al., 2007, Salmon et al., 2022, Mehta and Iyyani, 2024, Bargiacchi et al., 2024].

Over the last few decades, the angular distribution of GRB has been extensively examined [Meegan et al., 1992, Briggs et al., 1996, Balazs et al., 1998, Bernui et al., 2008, Magliocchetti et al., 2003, Cline et al., 2005, Vavrek et al., 2008, Gibelyou and Huterer, 2012, Li and Lin, 2015, Ukwatta and Wozniak, 2016, Tarnopolski, 2017].

Unlike several analyses on the isotropy of GRB, studies of the angular distribution of their radiative properties are less common. Nonetheless, two recent studies have examined the angular distribution of some GRB properties such as

duration, fluence, and peak flux in the FERMI dataset: Ripa and Shafieloo [2017] analyzed the sample with 1591 GRB from FERMI data, and Řípa and Shafieloo [2019] analyzed the sample with 2266 GRB from FERMI and ~2000 GRB from BATSE, finding a marginal anisotropic signature.

In this work, we use the latest FERMI/GBM dataset to analyze the angular and fluence distributions of the GRB on the celestial sphere, applying a coordinates-free method in spherical caps [Bernui et al., 2007, Kester et al., 2024]. Notice that the FERMI dataset does not provide information regarding the GRB redshift because, in general, it is not possible to observe these fast events with telescopes to perform spectroscopy of their visible counterpart. For this, all our analyses of the FERMIGRB catalogue concern the angular distribution of GRB events and their measured fluence. The current FERMIGRB catalogue comprises 3703 GRB from the FERMI/GBM instrument [Meegan et al., 2009]. In addition, we also consider the BATSE dataset [Paciesas et al., 1999b], which allows us to investigate possible systematic effects.

Our directional analysis is optimal for detecting preferred directions across the sky. Using this method, one can identify possible directional preferences in the angular distribution of GRB and in their fluence properties. The analysis of the angular distribution is based on the two-point angular correlation function (2PACF), while the directional analysis of their fluence is determined by the median of the fluence of the set of GRB in a given direction. Both the 2PACF and the median are computed in GRB samples within a specific spherical cap centered at a defined direction in the sky. The statistical significance in both cases is assessed by comparing the results with a large set of simulated ensembles produced under the SI hypothesis, where we apply the same directional analysis approach.

The outline of this work is as follows: In the next section, we briefly present the FERMI/GBM dataset and the samples used in this work. In Section 3, the method for the directional analysis of both the angular correlations and fluence of GRB is described, with details of the construction of

² T_{90} is the time, in seconds, to denote the duration over which a burst emits from 5% to 95% of its total measured counts [Koshut et al., 1996].

isotropy catalogues necessary to quantify possible SI deviations. Next, in Section 4, we present our results. Finally, in Section 5, we present our conclusions and final remarks. Consistency tests to determine the robustness of our findings are presented in the appendices.

2 The FERMI/GBM Burst Catalog

The study of the angular distribution of the GRB events started with the BATSE catalogues released at the end of the last century [Gehrels et al., 1993]. However, the investigation of the angular distribution of the GRB radiative properties is more recent, recognising the importance of these studies for a better comprehension of the stellar evolution in galaxies [Gruber et al., 2014, Hakila et al., 2000, Mehta and Iyyani, 2024].

2.1 Data selection

In our analyses, we use the current GRB catalogue from the FERMI Gamma-ray Burst Monitor instrument (FERMI/GBM)³ [von Kienlin et al., 2020], which is continuously being updated. In this study we used the version made available on February 2024, which contains 3703 GRB detected and their fluence measured; we will refer to this sample of 3703 GRB as the FERMIGRB catalogue.

For our studies, we make use of the following quantities of the FERMI GBM Burst catalogue: RA, right ascension; DEC, declination, both given in J2000 decimal degree units; Fluence, that is, flux integrated over the burst duration in erg cm^{-2} in the range 10–1000 keV energy band; and T_{90} .

To investigate the statistical isotropy of the FERMIGRB catalogue, we perform a directional analysis of the large-angle correlations in the celestial sphere. For this, we shall study three samples of GRB: the full FERMIGRB catalogue plus two sub-samples obtained by considering T_{90} as the division criterion: GRB with $T_{90} < 2$ s termed Short gamma-ray burst (SGRB), and GRB with $T_{90} > 2$ s termed Long gamma-ray burst (LGRB). The sky distribution of the FERMIGRB sample is shown in Figure 1; the analyses of the sub-

samples of SGRB and LGRB are presented in Appendix A, in particular, their sky distributions are shown in Figure 6.

In addition, we investigate the angular distribution of the fluence of the FERMIGRB sample, the fluence data of the FERMIGRB in the energy range of the BATSEGRB, i.e., 50–300 keV which we will refer to as the FERMI_{BAT} sample and, for the sake of comparison, of the fluence of the Fourth BATSE Gamma-Ray Burst Catalog⁴ [Paciesas et al., 1999a], which contains 1637 GRBs; however, for our analysis, we selected only the events for which the fluence was recorded simultaneously in all four channels GRB. In the case of the BATSE data, that we will refer to as the BATSEGRB sample, we use the fluence measurements obtained in four energy channels:

- Channel 1–BATSEGRB, with energy range 20–50 keV
- Channel 2–BATSEGRB, with energy range 50–100 keV
- Channel 3–BATSEGRB, with energy range 100–300 keV
- Channel 4–BATSEGRB, with energy range > 300 keV

3 Methodology

We describe the methodology adopted for the directional analysis that measures the large-scale angular correlations of the FERMIGRB sample, and also the directional analysis of the GRB fluence from FERMI and BATSE GRB catalogues.

3.1 Angular distribution of the GRB: σ -map

Our main goal is to search for possible preferred directions in the sky distribution of the FERMIGRB, and for this we study the intensity of their large-angle correlations. Our directional analysis is model independent and uses as estimator the 2PACF of Landy-Szalay (LS, Landy and Szalay [1993]; see also de Carvalho et al. [2020], Keihänen et al. [2019], Avila et al. [2019, 2021], Franco et al. [2024b]).

³<https://heasarc.gsfc.nasa.gov/W3Browse/fermi/fermigbrst.html>

⁴<https://heasarc.gsfc.nasa.gov/w3browse/all/batsegrb.html>

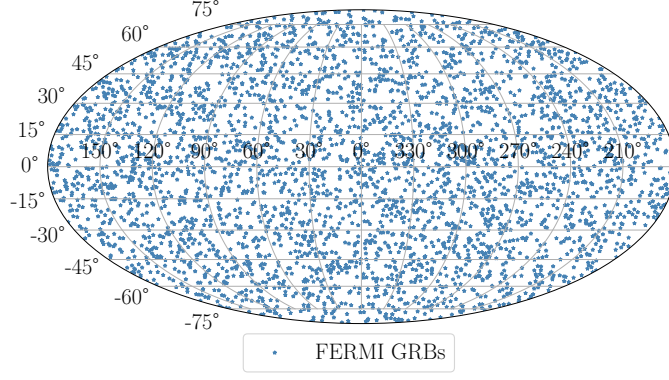


Figure 1: Distribution on the celestial sphere of 3703 GRB of the FERMIGRB catalogue (in Mollweide projection, in galactic coordinates).

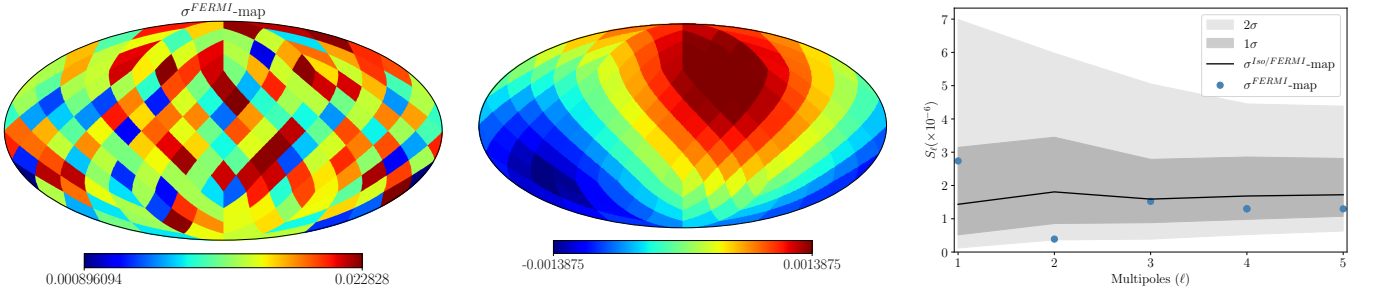


Figure 2: **Left panel:** The σ^{FERMI} -map, with resolution $N_{\text{side}}=4$, obtained from the directional analyses of the FERMIGRB sample. **Middle panel:** The corresponding dipole component of the σ^{FERMI} -map. **Right panel:** Power spectrum $\mathcal{S}_\ell^{\text{FERMI}}$, $\ell = 1, \dots, 5$ of the σ^{FERMI} -map shown as dots in steel blue color, and the median power spectrum of 500 isotropic σ -maps are shown on the solid line. The shaded region corresponds to 1σ and 2σ deviations from the isotropic case.

Let us define a spherical cap, with radius equal to γ , centered in the J pixel with angular coordinates (θ_J, ϕ_J) as

$$\Omega_\gamma^J \equiv \Omega(\theta_J, \phi_J; \gamma) \subset \mathcal{S}^2, \quad (1)$$

where \mathcal{S}^2 represents the celestial sphere, and J is the index of the cap in analysis, with $J = 1, \dots, N_{\text{caps}}$. Notice that an hemisphere is a spherical cap with $\gamma = 90^\circ$. In each one of these caps, the 2PACF is computed using the LS estimator

$$\omega(\theta)^J \equiv \frac{DD(\theta) - 2DR(\theta) + RR(\theta)}{RR(\theta)}, \quad (2)$$

with $\theta \in \langle 0, 2\gamma \rangle$ ⁵; $DD(\theta)$ is the number of GRB pairs in the sample data with angular separation θ , normalized by the total number of pairs; $RR(\theta)$ is a similar quantity, but for the pairs in a random simulated sample; and $DR(\theta)$ corresponds

to a cross-correlation between a data object and a random object. Our directional analysis only use the measured angular coordinates, i.e., the sky position, of the GRB event to calculate the angular distance between pairs, which is given by

$$\theta_{ij} = \cos^{-1}[\sin(\delta_i) \sin(\delta_j) + \cos(\delta_i) \cos(\delta_j) \cos(\alpha_i - \alpha_j)], \quad (3)$$

where α_i, α_j and δ_i, δ_j are the right ascension and the declination, respectively, of the GRB i and j .

We denote by $\omega_k^J \equiv \omega(\theta_k)^J$ the 2PACF value, in the J -th spherical cap, for the angular distances $\{\theta_{ij}\}$ in the interval $\theta_{ij} \in \theta_k \equiv \langle (k-1)\beta, k\beta \rangle$ for $k = 1, \dots, N_{\text{bins}}$, where $N_{\text{bins}} \equiv 2\gamma/\beta$ is the number of bins and β is the bin length. We adopt $\gamma = 90^\circ$ and $N_{\text{bins}} = 35$ in our analyses. The number of caps, N_{caps} , depends on the pixelization parameter N_{side} ; we adopt $N_{\text{side}} = 4$ which means $N_{\text{caps}} = 192$; we denote by $\{n_J\}$, for $J = 1, \dots, 192$, the number of GRB in the set of

⁵Notice that the symbol $\langle \dots, \dots \rangle$ means that the interval is open by the left and closed by the right.

192 hemispheres (i.e., $\gamma = 90^\circ$).

We must note that the function $\omega = \omega(\theta)^J$ measures the 2PACF in a given direction, specifically, it encompasses the information regarding the angular correlations produced by the distribution of the cosmic objects in the J -th spherical cap. The next step is to quantify the difference between angular correlations observed in different directions. In order to do this we use the σ -map method [Bernui et al., 2008, Kester et al., 2024]. The σ -map is a model-independent approach useful to detect preferred directions in data displayed on a sphere, evidencing different angular correlations intensities, analysis done through the 2PACF on spherical caps that scan the celestial sphere and then compare the observational data results with the same procedure applied to synthetic SI maps. Our σ -maps are celestial maps of 192 real values, then converted in coloured maps, containing information of the angular correlations intensity in each region of the celestial sphere analysed. To quantify the directional variation of the correlation intensity, we define a scalar function to associate a non negative real value to each spherical cap with center in (θ_J, ϕ_J) , that is

$$\sigma_J : \Omega_\gamma^J \subset \mathcal{S}^2 \mapsto \mathbb{R}^+, \quad (4)$$

for $J = 1, \dots, N_{\text{caps}}$, where our estimator σ_J is defined by

$$\sigma_J^2 \equiv \frac{1}{N_{\text{bins}}} \sum_{k=1}^{N_{\text{bins}}} (\omega_k^J)^2, \quad (5)$$

with $\sigma_J = \sigma_J(\theta_J, \phi_J)$. Then, the set of real positive numbers $\{\sigma_J^2\}$, for $J = 1, \dots, N_{\text{caps}}$, is the σ -map. To detect any possible preferred direction or asymmetry we perform the spherical harmonics decomposition

$$\sigma^2(\theta, \phi) = \sum_{\ell m} a_{\ell m}^\sigma Y_{\ell m}(\theta, \phi), \quad (6)$$

and analyze its angular power spectrum

$$\mathcal{S}_\ell \equiv \frac{1}{2\ell + 1} \sum_{m=-\ell}^{\ell} |a_{\ell m}^\sigma|^2. \quad (7)$$

The distribution of values of the σ -map power spectra, $\{\mathcal{S}_\ell\}$, obtained from a similar directional analysis applied to a set of simulated SI GRB

maps, helps us to quantify how frequent or rare the multipoles \mathcal{S}_ℓ of the FERMIGRB σ -map are. A dipolar pattern of the map or a large value for the dipole \mathcal{S}_1 , for instance, could indicate the presence of a preferred axis in the sky, that is, a possible isotropy violation in the angular distribution of the FERMIGRB. This makes necessary the evaluation of the statistical significance of the angular power spectra $\{\mathcal{S}_\ell\}$ at large angles, i.e., $\ell = 1, \dots, 5$.

3.2 Angular distribution of the GRB fluence: f -map

To quantify the directional variation of the fluence of the GRB sample in analysis, we consider the GRB in the J -th spherical cap, with center in (θ_J, ϕ_J) , and define a scalar function to associate a non negative real value, that is

$$\bar{F}_J : \Omega_\gamma^J \subset \mathcal{S}^2 \mapsto \mathbb{R}^+, \quad (8)$$

for $J = 1, \dots, N_{\text{caps}}$, where \bar{F}_J is defined as the median fluence

$$\bar{F}_J \equiv \text{median}[\{F_i\}_J], \quad (9)$$

being $\{F_i\}_J$ the set of fluences of the GRB located in the J -th spherical cap.

The set of N_{caps} values: $\{\bar{F}_J\}$, for $J = 1, \dots, N_{\text{caps}}$, is then assembled together into a full-sky map, hereafter the fluence-map or f -map.

Then, this map is decomposed in spherical harmonics and its angular power spectrum analyzed as usual

$$\mathcal{F}_\ell \equiv \frac{1}{2\ell + 1} \sum_{m=-\ell}^{\ell} |a_{\ell m}^{\bar{F}}|^2. \quad (10)$$

Finally, the evaluation of the statistical significance of the angular power spectrum $\{\mathcal{F}_\ell\}$ provides us with a measure of the possible isotropy deviations, at several scales, of the angular distribution of the GRB fluence.

3.3 Simulating isotropic σ -maps and f -maps

An important part of our directional analysis is the evaluation of the multipole features of the σ -maps and f -maps. This is done by quantifying their angular power spectra and comparing them with those spectra computed from large sets

of $\{\sigma^{\text{ISO}}\}$ -maps and $\{f^{\text{ISO}}\}$ -maps produced under the SI hypothesis and according to the following procedures.

Firstly, remember that in the FERMIGRB catalogue, the set of numbers of GRB in each hemisphere is given by $\{n_J\}$, $J = 1, \dots, 192$, corresponding to 192 hemispheres. For the σ -map analyses, we first generate a random catalogue with 100 000 objects uniformly distributed on the celestial sphere, that is, considering $\alpha \in [0^\circ, 360^\circ]$ and $\delta \in [-90^\circ, 90^\circ]$ (see, e.g. [Franco et al. \[2024a\]](#)). From this dataset we randomly select n_J simulated cosmic objects for the J -th hemisphere, then we obtain the set of numbers $\{n_J\}$ for the 192 hemispheres. Next, we apply our directional analysis to this ensemble obtaining one σ^{ISO} -map. For the 2PACF analyses in each hemisphere we use the code *TreeCorr*⁶ written in python language. In brief, this procedure corresponds to the analysis of one simulated SI GRB sky distribution, providing one σ^{ISO} -map. We repeat this procedure 500 times, producing a set of 500 σ^{ISO} -maps; then we compute the angular power spectra of each one of these maps. The resulting power spectra are shown in the right panel of Figure 2, where the median spectrum is represented as a continuous line, and the 1σ , 2σ uncertainty regions are represented as shadow regions. A similar procedure of analysis was performed with the SGRB and LGRB sub-samples in Appendix A, generating 500 $\sigma^{\text{ISO/SGRB}}$ -maps and 500 $\sigma^{\text{ISO/LGRB}}$ -maps, respectively.

To produce the set of f^{ISO} -maps we follow a different procedure. We keep the angular positions of each GRB, (α_i, δ_i) , therefore preserving the quantity of GRB in each hemisphere, $\{n_J\}$. We then perform the isotropization of the fluence dataset $\{F_i\}$ in two steps: $F_i \xrightarrow{\text{rand.}} F_i^{\text{ran}} \xrightarrow{\text{Gaus.}} F_i^{\text{ran+Gau}}$; in brief: we first randomize the original dataset obtaining $\{F_i^{\text{ran}}\}$, then each of these values is changed by a value randomly selected from a Gaussian distribution with mean F_i^{ran} and standard deviation equal to its measured uncertainty $\sigma_{F_i^{\text{ran}}}$, obtaining $\{F_i^{\text{ran+Gau}}\}$. The set of triplets $\{(\alpha_i, \delta_i, F_i^{\text{ran+Gau}})\}$, $i = 1, \dots, 3703$, form one simulated catalogue, generated under the SI hypothesis, that after applying our directional analysis procedure produces one f^{ISO} -map. We repeat this procedure to finally obtain 500 f^{ISO} -

maps.

4 Analyses and results

We applied the methodology described in the previous section to the FERMIGRB catalogue. The results of the directional analysis are discussed separately: first, we analyze the angular distribution of the GRB, and then, their fluence distribution. In both cases, the statistical significance was evaluated by comparison with similar analyses applied to isotropic Monte Carlo catalogues (σ^{ISO} -maps and f^{ISO} -maps) constructed as described above (see Sec. 3.3). Such analyses allowed us to quantify the significance level of our findings and to evaluate whether the distribution of GRB and their respective fluences are isotropic.

4.1 GRB distribution on the sky

We investigate the large-angle distribution of GRB on the sky. This is done through the analysis of the intensity of the angular correlations in several directions along the celestial sphere, as explained in section 3.1.

We first calculate the σ -map for the full GRB sample, σ^{FERMI} -map. Our result is displayed in the left panel of Figure 2, where it can be seen that there is no excess or deficit of correlation around any particular direction. In other words, correlation intensities are isotropically distributed around the sky. In the middle panel we show the σ^{FERMI} -map dipolar component. Next, we quantify the significance of the large-angle multipoles, through a comparison with a set of 500 SI σ -maps. To do this, we generate a set of 500 simulated SI GRB catalogues and apply the same directional analysis methodology to each one, obtaining a set of 500 σ^{ISO} -maps. Then, we calculate their angular power spectra \mathcal{S}_ℓ , for $\ell = 1, \dots, 5$. Finally, we compare the spectral angular signatures of the σ^{FERMI} -map, i.e., $\mathcal{S}_\ell^{\text{FERMI}}$, with these SI spectra. The result is displayed in the right panel of Figure 2, where $\mathcal{S}_\ell^{\text{FERMI}}$ is represented by blue dots, the black line represents the median value of the set $\{\mathcal{S}_\ell^{\text{ISO}}\}$; the 1σ and 2σ regions are shown as shadows in gray. We observe that the σ^{FERMI} -map is compatible with the SI hypothesis, within 1σ confidence level, at all the large-angles ana-

⁶https://rmjarvis.github.io/TreeCorr/_build/html/overview.html.

lyzed. Moreover, as a consistency test, we analyze the angular distribution for the SGRB and LGRB subsamples, discussion presented in the Appendix A.

4.2 GRB Fluence distribution on the sky

To investigate the angular distribution of the FERMIGRB fluence, we used the f -maps described in Section 3.2. The f -maps allow for a directional investigation of the fluence’s angular distribution across the sky, and their power spectrum, \mathcal{F}_ℓ , helps us better quantify the statistical significance of our findings. Figure 3 presents the f^{FERMI} -map for the FERMIGRB catalogue (left panel) and its dipolar component (middle panel). The power spectrum, $\mathcal{F}_\ell^{\text{FERMI}}$, shown in the right panel (blue dots) for $\ell = 1, \dots, 5$, evidences that the f^{FERMI} -map is highly dominated by its dipolar component and differently from the σ^{FERMI} -map, it shows a clear dipole structure, as seen in Figure 3 (left panel). To evaluate the statistical significance of the multipolar components of the f -maps, we compared them with SI f^{ISO} -maps. To this end, we computed the f -map angular power spectrum for a set of 500 simulated SI f^{ISO} -maps, whose median is shown in the right panel of Figure 3 (black line), alongside the 1σ and 2σ regions in gray. We clearly note that, although the dipole behavior is remarkable, it is not anomalous compared to the isotropic case; in fact, the analysis of the angular power spectra shows that the f^{FERMI} -map is essentially a dipole.

The dipole component from the FERMIGRB catalogue indicates a net preference for the galactic plane region, at approximately $(l, b) \simeq (268^\circ, -3^\circ) \pm (11.2^\circ, 11.2^\circ)$. To investigate a possible bias in our results, we studied the correlation of our outcomes with GRB located in the galactic plane. Thus, we removed the data located in the galactic region and redo the analyses. This involved applying a cut to the region of avoidance with a range $|b| \leq 20^\circ$ in galactic coordinates, which excluded 33% of the sky. The left panel in Figure 4 shows the distribution of GRB after applying this galactic cut. After the cut, we computed the new $f^{\text{FERMI},\text{mkd}}$ -map, and the result is presented in Figure 4 (left panel), where its dipolar component is also shown (mid-

dle panel). The angular features and the dipolar pattern in the fluence distribution previously found analysing the full-sky data remain (right panel). This result indicates that there is no appreciable correlation between the GRB fluence localized in the galactic plane and the dipole direction found in f^{FERMI} -map.

So far, we have presented in this section the analysis of the fluence of the FERMIGRB sample considering $\gamma = 90^\circ$. In Appendix B, we conducted robustness tests for the directional analysis, this time considering different sizes of the spherical cap, namely $\gamma = 45^\circ, 60^\circ, 65^\circ, 70^\circ$. As shown in Appendix B, the dipolar pattern is consistent in all cases (see Table 1).

Additionally, we investigated possible instrumental, systematic or data-processing effects biasing our fluence results. To do this, we conducted two types of additional analyses. Firstly, we evaluated possible correlations between our findings and the number of GRB in each hemisphere using the linear Pearson correlation coefficient. The results, presented in the Appendix C, indicate no significant correlation. Second, we applied a similar directional analysis to the BATSE dataset. BATSE experiment operated in four channels, with the energy intervals described in Section 2. For comparison with the BATSE dataset, we constructed a subsample of the FERMIGRB catalogue in a similar energy range as BATSE data. The results are very similar to those displayed in Figure 3 for the full FERMIGRB sample (see Appendix D), confirming the robustness of our findings.

5 Conclusions

An important issue of the standard cosmological model is to establish the universe large-scale properties, that is, to know how matter and radiation are distributed at large scales in the observed universe [Tarnopolski, 2017, Dainotti et al., 2022, Sorrenti et al., 2024b,a, Lopes et al., 2024]. In this regard, the updated catalogues of GRB are a valuable source of astrophysical information to inquire if such energetic events are in fact universal astrophysical processes happened everywhere and at any epoch of the universe. We have investigated the large angular distribution on the celestial sphere of the latest FERMIGRB cata-

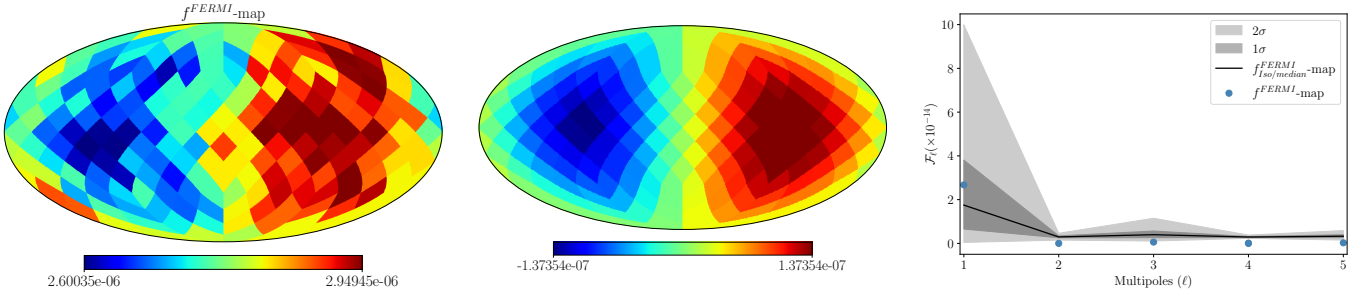


Figure 3: **Left panel:** The f^{FERMI} -map for the FERMIGRB catalogue. **Middle panel:** The dipole component of the f^{FERMI} -map. **Right panel:** The power spectrum of the f^{FERMI} -map. Note that fluence-maps are in units erg/cm^2 , in galactic coordinates system, and with resolution $N_{\text{side}} = 4$.

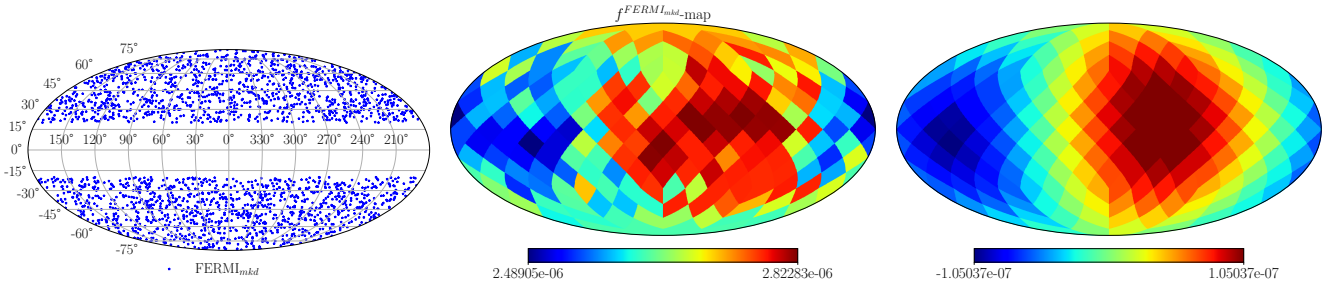


Figure 4: **Left panel:** Distribution of GRB on the celestial sphere of the FERMIGRB-Masked sample, showing 2428 GRB, where we implemented a cut of the zone of avoidance removing GRB with $|b| \leq 20^\circ$ (in galactic coordinates). **Middle and Right panels:** The f -map with resolution $N_{\text{side}} = 4$ (middle panel) and its dipole component (right panel) for the FERMIGRB-Masked. Note that all these maps above are in units erg/cm^2 and in galactic coordinates system.

logue, and of their fluence property, applying a model-independent approach. Although the first problem has been extensively studied, the latter received less attention [Ripa and Shafieloo, 2017, Řípa and Shafieloo, 2019].

In summary, we found a highly isotropic distribution of GRB, both in FERMIGRB catalogue and in sub-samples SGRB and LGRB (see appendix A). This indicates that, on average, the GRB observed by FERMI and their host galaxies are not anomalously clustered. This reinforces their extra-galactic origin at cosmological scales and supports the idea that these universal astrophysical processes occur everywhere and at any epoch in the universe.

Moreover, the directional analysis of the fluence data shows a net dipolar pattern for the FERMIGRB, FERMI_{BAT}, and BATSE Channel 4 catalogs, as revealed by their corresponding angular power spectra (see the right panels in Figures 3 and 4, and the analyses in Appendix D), where they appear with low statistical significance, \sim

1σ , suggestive of SI. The dipole behaviour observed in the f -maps of the analyzed catalogues, with their dipole direction close to the galactic plane for the FERMIGRB and FERMI_{BAT} data, motivates further consistency analyses to investigate possible systematics. Thus, we study the possible correlation with the data located around the Milky Way galactic plane or a possible influence of the number of GRB observed in each sky patch. Nevertheless, as shown in Figure 4 and Appendix C, we did not find a substantial correlation for attributing to these effects the cause of the dipole pattern.

The positive dipole directions in the cases studied in this work are summarized in Figure 5.

Intriguingly, the f -map from BATSE Channel 4 data shows a net dipolar pattern with the dipole direction aligned with the direction of the cosmic microwave background dipole [Javanmardi et al., 2015, Singal, 2019, Luongo et al., 2022, Krishnan et al., 2022, Zhai and Percival, 2022, Mittal et al., 2024], as shown in Table 3 and in Appendix D, al-

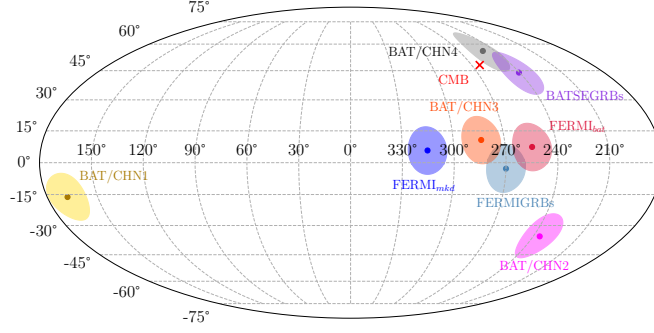


Figure 5: Mollweide projection, in galactic coordinates, of the dipole directions from f -map analyses, as displayed in Table 3. The shaded regions corresponds to 1σ uncertainties. The labels identify the samples in analysis; the abbreviations means: BAT for *BATSE* data, MSK for *masked* map, and CHN for *channel* in analysis.

though its statistical significance is not high (see Figure 9).

Acknowledgments

M.L. and C.F. acknowledge to CAPES, A.B. acknowledges to CNPq, for their corresponding fellowships. W.S.H.R., thanks to FAPES (PRONEM No 503/2020) for the financial support under which this work was carried out. F.A. thanks to CNPq and FAPERJ, Processo SEI 260003/014913/2023, for the financial support.

A Consistency test: the SI of FERMI LGRB and SGRB samples

In this appendix, we study the angular distribution of the Short- (SGRB) and Long-GRB (LGRB) samples following the same directional analysis approach, applied to the full FERMIGRB sample (with 3703 GRB) in section 4.1.

Regarding the angular distribution of the SGRB and LGRB samples, the literature reports analyses of different catalogues using a variety of methodologies (see, e.g., Balazs et al. [1998], Magliocchetti et al. [2003], Bernui et al. [2008], Ukwatta and Wozniak [2016], Ripa and Shafieloo [2017], Řípa and Shafieloo [2019], Tarnopolski [2017]). For this, we find interesting to test the hypothesis of SI for each of these sub-samples from the updated FERMIGRB catalogue. In this case, the number of GRB in the SGRB and LGRB samples is 614 and 3089, respectively. The sky distribution of these samples can be seen in the Mollweide projection presented in Figure 6.

Our results are displayed in Figure 7. From left to right in the first (second) row, we show the analyses for the SGRB (LGRB) sample, that is the σ^{SGRB} -map (σ^{LGRB} -map), its dipole, and its angular power spectrum $\mathcal{S}_\ell^{\text{SGRB}}$ ($\mathcal{S}_\ell^{\text{LGRB}}$) for $\ell = 1, \dots, 5$.

More precisely, the right panels in both rows of Figure 7 compare the data power spectra, $\mathcal{S}_\ell^{\text{SGRB}}$ and $\mathcal{S}_\ell^{\text{LGRB}}$ (dots), with the corresponding sets of power spectra obtained from synthetic σ^{ISO} -maps. These σ -maps were produced from two sets of 500 simulated isotropic maps for each case, i.e., SGRB and LGRB. The continuous line represents the median power spectrum, and the shaded areas represent the 1σ and 2σ statistical confidence levels, respectively. The results are consistent with those found in Section 4.1. For completeness, we also study the f -maps of the SGRB and LGRB samples, although the corresponding figures are not displayed. In both cases, the analyses show that these f -maps are also compatible with the SI hypothesis.

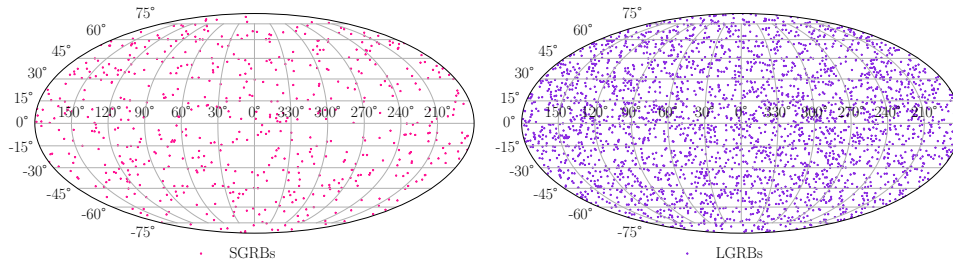


Figure 6: Angular distribution in galactic coordinates, in Mollweide projection, of the sub-samples of 614 SGRB (left panel) and 3089 LGRB (right panel) from FERMI catalogue.

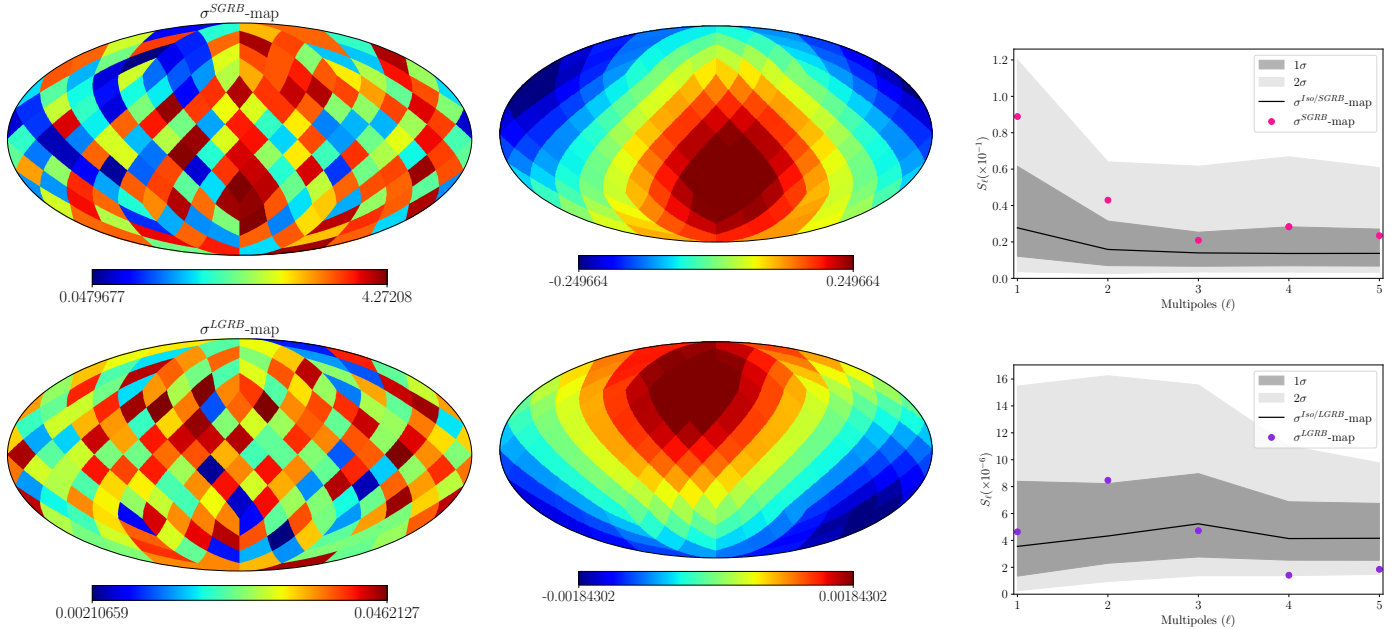


Figure 7: The first/second row corresponds to the SGRB/LGRB angular distribution analyses. **Left panel:** The $\sigma^{\text{SGRB/LGRB}}$ -map obtained from the directional analyses of the SGRB and LGRB samples. **Middle panel:** The corresponding dipole component of the $\sigma^{\text{SGRB/LGRB}}$ -map. **Right panel:** Power spectrum $\mathcal{S}_\ell^{\text{SGRB/LGRB}}$, $\ell = 1, \dots, 5$ of the $\sigma^{\text{SGRB/LGRB}}$ -map shown as dots, and the median power spectrum of 500 isotropic σ -maps are shown on the solid line. The shaded region corresponds to 1σ and 2σ deviations from the isotropic case.

B Consistency test: spherical cap size

In this appendix we perform isotropy analyses of the f -maps considering spherical cap sizes, namely $\gamma = 45^\circ, 60^\circ, 65^\circ, 70^\circ$ (see Table 1).

These results support our previous conclusions regarding the isotropic distribution of GRB.

C Directional variation of the number of GRB and the f -map signatures

In this Appendix, we investigate the possible correlation between the number of GRB with the directional signatures of the f -maps. For this, we perform a correlation analysis of the number-of-GRB-map (that is, the map where the color in each pixel represents the number of GRB used to construct our σ -map or the f -maps, see Figure 8) with the σ -map and with the f -maps, using the linear Pearson correlation coefficient \mathcal{P} . Our analyses are summarized in Table 2. According to the literature, for values of the Pearson coefficient in the interval (the vertical bars mean absolute value),

$\gamma(^{\circ})$	$l \pm 11.2, (^{\circ})$	$b \pm 11.2, (^{\circ})$
90	268.02	-2.80
45	267.63	4.86
60	266.01	-2.66
65	266.85	-2.38
70	265.99	-4.36

Table 1: Dipole directions for the f^{FERMI} -maps obtained from FERMIGRB full sample and different spherical cap sizes.

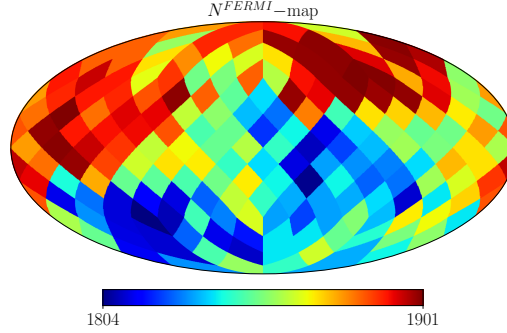


Figure 8: Number-of-GRB-map from sample FERMI, or N^{FERMI} -map, shown in Mollweide projection and galactic coordinates, to study the correlation analyses with the f^{FERMI} -maps (see Appendix C for details).

$|\mathcal{P}| \in [0.0, 0.19]$ means that the linear correlation between the pair of maps is *very low*; for values $|\mathcal{P}| \in [0.6, 0.79]$ the correlation between the pair of maps is *high*; while for values $|\mathcal{P}| \in [0.8, 1.0]$ the correlation between the pair of maps is *very high*.

According to these results, we conclude that the N -map, i.e., the number-of-GRB-map, that quantifies the number of GRB in each spherical cap, has a negligible correlation with the angular signatures found in the f^{FERMI} -map.

	$f^{\text{FERMI}}\text{-map}$	$f^{\text{FERMI}}_{\text{mkd}}\text{-map}$	$f^{\text{FERMI}}_{\text{bat}}\text{-map}$
$N\text{-map}$	-0.076	-0.170	0.078
$f^{\text{FERMI}}\text{-map}$	—	0.672	0.941

Table 2: Correlation analyses: Pearson coefficient calculated to study the linear correlation between different maps. For instance, the value -0.170 means that the N -map is weakly anti-correlated with the $f^{\text{FERMI, cut}}\text{-map}$.

D Statistical Isotropy analyses of FERMIGRB Fluence in BATSE Channels

Additionally, we study the statistical isotropy of the FERMIGRB fluence in the BATSE Channels. The power spectrum shown in the right panel of Figure 9 confirms the SI at 1σ confidence level, a fully similar result presented in Figure 3 corresponding to the statistical analyses of the FERMIGRB catalogue. Our results for the dipole directions of these analyses are summarized in Table 3, and illustrated in Figure 5.

In Table 3 we present the direction, in galactic coordinates, along which the fluence dipole appears. In Figure 5 we illustrate all those directions in a Mollweide celestial sphere projection.

We also show, in Figure 10, the histograms of the fluence data for the catalogues analysed.

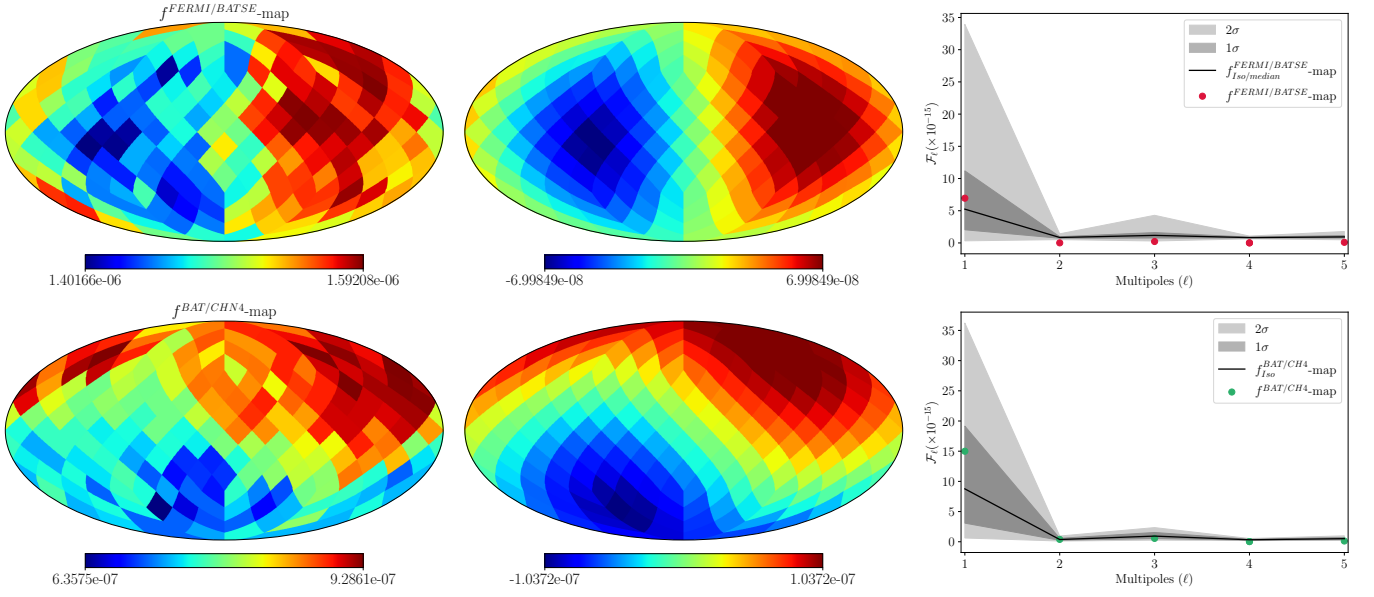


Figure 9: The FERMI-BATSE analyses of the fluence angular distribution. **Left panel:** The $f^{FERMI-Batse}_{map}$ for the FERMI-BATSE catalogue. **Middle panel:** The dipole component of the $f^{FERMI-Batse}_{map}$. **Right panel:** The power spectrum of the $f^{FERMI-Batse}_{map}$.

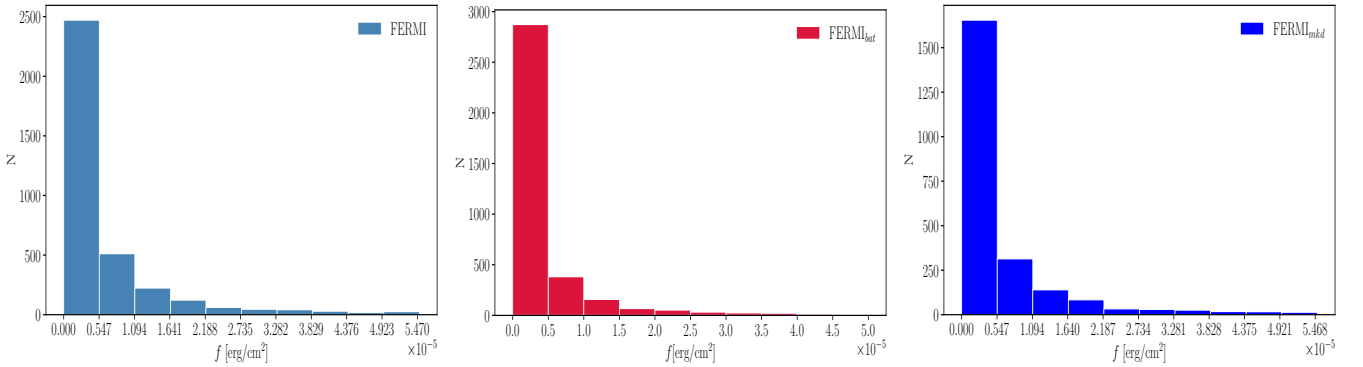


Figure 10: **Left panel:** Frequency histogram of the measured fluence for the sample of 3691 FERMI-GRB, the bin size is $\Delta\mathcal{F} \simeq 3.02 \times 10^{-5} [\text{erg}/\text{cm}^2]$, in the energy band, nominally 10-1000 keV. For visualization purposes, 12 GRB were removed from the original sample of 3703 GRB. **Middle panel:** Frequency histogram of the the FERMI-GRB_{bat} sample in the BATSE standard energy band, nominally 50-300 keV. **Right panel:** Frequency histogram of the 2428 GRB remaining of the original FERMI-GRB sample (left panel) after we remove the GRB located in the Zone of Avoidance, that is, those GRB with $|b| \leq 20^\circ$ (i.e., $-20^\circ \leq \text{DEC} \leq +20^\circ$, see Figure 4).

Sample	$l \pm 11.2$ ($^{\circ}$)	$b \pm 11.2$ ($^{\circ}$)
FERMIGRB	268.02	−2.80
FERMI _{MKD}	315.33	5.73
FERMI _{BAT}	254.41	7.39
BAT/CHN1	167.96	−16.19
BAT/CHN2	235.72	−35.45
BAT/CHN3	283.60	10.69
BAT/CHN4	249.99	55.92
BATSEGRB	240.46	43.97

Table 3: Dipole directions for the f -maps obtained from different samples, with hemispheres $\gamma = 90^{\circ}$. The locations on the celestial sphere are shown in Figure 5.

References

- Y. Akrami et al. Planck 2018 results. VII. Isotropy and Statistics of the CMB. *A&A*, 641:A7, 2020. doi: 10.1051/0004-6361/201935201.
- P. K. Aluri, P. Cea, P. Chingangbam, M.-C. Chu, R. G. Clowes, D. Hutsemékers, J. P. Kochappan, A. M. Lopez, L. Liu, N. C. M. Martens, C. J. A. P. Martins, K. Migkas, E. Ó Colgáin, P. Pranav, L. Shamir, A. K. Singal, M. M. Sheikh-Jabbari, J. Wagner, S.-J. Wang, D. L. Wiltshire, S. Yeung, L. Yin, and W. Zhao. Is the observable Universe consistent with the cosmological principle? *Classical and Quantum Gravity*, 40(9):094001, May 2023. doi: 10.1088/1361-6382/acbefc.
- F. Avila, C. P. Novaes, A. Bernui, E. de Carvalho, and J. P. Nogueira-Cavalcante. The angular scale of homogeneity in the local Universe with the SDSS blue galaxies. *MNRAS*, 488(1):1481–1487, Sept. 2019. doi: 10.1093/mnras/stz1765.
- F. Avila, A. Bernui, E. de Carvalho, and C. P. Novaes. The growth rate of cosmic structures in the local Universe with the ALFALFA survey. *MNRAS*, 505(3):3404–3413, Aug. 2021. doi: 10.1093/mnras/stab1488.
- L. G. Balazs, A. Meszaros, and I. Horvath. Anisotropy of the sky distribution of gamma-ray bursts. *A&A*, 339:1, 1998.
- G. Bargiacchi, M. G. Dainotti, and S. Capozziello. High-redshift Cosmology by Gamma-Ray Bursts: an overview. *arXiv e-prints*, art. arXiv:2408.10707, Aug. 2024. doi: 10.48550/arXiv.2408.10707.
- A. Bernui and W. S. Hipolito-Ricaldi. Can a primordial magnetic field originate large-scale anomalies in WMAP data? *MNRAS*, 389:1453–1460, 2008. doi: 10.1111/j.1365-2966.2008.13683.x.
- A. Bernui, B. Mota, M. J. Rebouças, and R. Tavakol. a Note on the Large-Angle Anisotropies in the Wmap Cut-Sky Maps. *International Journal of Modern Physics D*, 16(2-03):411–420, Jan. 2007. doi: 10.1142/S0218271807010195.
- A. Bernui, I. S. Ferreira, and C. A. Wuensche. On the Large-Scale Angular Distribution of Short Gamma-Ray Bursts. *ApJ*, 673(2):968–971, Feb. 2008. doi: 10.1086/524678.
- M. S. Briggs, W. S. Paciesas, G. N. Pendleton, C. A. Meegan, G. J. Fishman, J. M. Horack, M. N. Brock, C. Kouveliotou, D. H. Hartmann, and J. Hakkila. BATSE Observations of the Large-Scale Isotropy of Gamma-Ray Bursts. *ApJ*, 459:40, Mar. 1996. doi: 10.1086/176867.

- D. B. Cline, B. Czerny, C. Matthey, A. Janiuk, and S. Otwinowski. Study of very short grb: new results from batse and konus. *Astrophys. J. Lett.*, 633:L73–L76, 2005. doi: 10.1086/498567.
- J. Colin, R. Mohayaee, S. Sarkar, and A. Shafieloo. Probing the anisotropic local Universe and beyond with SNe Ia data. *MNRAS*, 414(1):264–271, June 2011. doi: 10.1111/j.1365-2966.2011.18402.x.
- M. G. Dainotti, V. Nielson, G. Sarracino, E. Rinaldi, S. Nagataki, S. Capozziello, O. Y. Gnedin, and G. Bargiacchi. Optical and X-ray GRB Fundamental Planes as cosmological distance indicators. *MNRAS*, 514(2):1828–1856, Aug. 2022. doi: 10.1093/mnras/stac1141.
- E. de Carvalho, A. Bernui, H. S. Xavier, and C. P. Novaes. Baryon acoustic oscillations signature in the three-point angular correlation function from the SDSS-DR12 quasar survey. *MNRAS*, 492(3):4469–4476, Mar. 2020. doi: 10.1093/mnras/staa119.
- A. de Oliveira-Costa, M. Tegmark, M. Zaldarriaga, and A. Hamilton. The Significance of the largest scale CMB fluctuations in WMAP. *Phys. Rev. D*, 69:063516, 2004. doi: 10.1103/PhysRevD.69.063516.
- H. K. Eriksen, F. K. Hansen, A. J. Banday, K. M. Gorski, and P. B. Lilje. Asymmetries in the Cosmic Microwave Background anisotropy field. *Astrophys. J.*, 605:14–20, 2004. doi: 10.1086/382267. [Erratum: *Astrophys. J.* 609, 1198 (2004)].
- G. J. Fishman, C. A. Meegan, R. B. Wilson, M. N. Brock, J. M. Horack, C. Kouveliotou, S. Howard, W. S. Paciesas, M. S. Briggs, G. N. Pendleton, T. M. Koshut, R. S. Mallozzi, M. Stollberg, and J. P. Lestrade. The First BATSE Gamma-Ray Burst Catalog. *ApJs*, 92:229, May 1994. doi: 10.1086/191968.
- C. Franco, F. Avila, and A. Bernui. Probing cosmic isotropy in the Local Universe. *MNRAS*, 527(3):7400–7413, Jan. 2024a. doi: 10.1093/mnras/stad3616.
- C. Franco, J. Oliveira, M. Lopes, F. Avila, and A. Bernui. Measuring the matter fluctuations in the Local Universe with the ALFALFA catalog. *arXiv e-prints*, art. arXiv:2406.16693, June 2024b. doi: 10.48550/arXiv.2406.16693.
- N. Gehrels, E. Chipman, and D. A. Kniffen. The Compton Gamma Ray Observatory. *A&As*, 97: 5–12, Jan. 1993.
- C. Gibelyou and D. Huterer. Dipoles in the Sky. *Mon. Not. Roy. Astron. Soc.*, 427:1994–2021, 2012. doi: 10.1111/j.1365-2966.2012.22032.x.
- D. Gruber, A. Goldstein, V. Weller von Ahlefeld, P. Narayana Bhat, E. Bissaldi, M. S. Briggs, D. Byrne, W. H. Cleveland, V. Connaughton, R. Diehl, G. J. Fishman, G. Fitzpatrick, S. Foley, M. Gibby, M. M. Giles, J. Greiner, S. Guiriec, A. J. van der Horst, A. von Kienlin, C. Kouveliotou, E. Layden, L. Lin, C. A. Meegan, S. McGlynn, W. S. Paciesas, V. Pelassa, R. D. Preece, A. Rau, C. A. Wilson-Hodge, S. Xiong, G. Younes, and H.-F. Yu. The Fermi GBM Gamma-Ray Burst Spectral Catalog: Four Years of Data. *ApJs*, 211(1):12, Mar. 2014. doi: 10.1088/0067-0049/211/1/12.
- J. Hakkila, D. J. Haglin, G. N. Pendleton, R. S. Mallozzi, C. A. Meegan, and R. J. Roiger. Gamma-Ray Burst Class Properties. *ApJ*, 538(1):165–180, July 2000. doi: 10.1086/309107.
- J. Hakkila, T. W. GIBLIN, K. C. Young, S. P. Fuller, C. D. Peters, C. Nolan, S. M. Sonnett, D. J. Haglin, and R. J. Roiger. A Gamma-Ray Burst Database of BATSE Spectral Lag and Internal Luminosity Function Values. *ApJs*, 169(1):62–74, Mar. 2007. doi: 10.1086/511306.

- W. S. Hipolito-Ricaldi and G. I. Gomero. Topological signatures in CMB temperature anisotropy maps. *Phys. Rev. D*, 72:103008, 2005. doi: 10.1103/PhysRevD.72.103008.
- K. T. Inoue and J. Silk. Local Voids as the Origin of Large-Angle Cosmic Microwave Background Anomalies. I. *ApJ*, 648(1):23–30, Sept. 2006. doi: 10.1086/505636.
- B. Javanmardi, C. Porciani, P. Kroupa, and J. Pflamm-Altenburg. Probing the Isotropy of Cosmic Acceleration Traced By Type Ia Supernovae. *ApJ*, 810(1):47, Sept. 2015. doi: 10.1088/0004-637X/810/1/47.
- E. Keihänen, H. Kurki-Suonio, V. Lindholm, A. Viitanen, A. S. Suur-Uski, V. Allevato, E. Branchini, F. Marulli, P. Norberg, D. Tavagnacco, S. de la Torre, J. Valiviita, M. Viel, J. Bel, M. Frailis, and A. G. Sánchez. Estimating the galaxy two-point correlation function using a split random catalog. *A&A*, 631:A73, Nov. 2019. doi: 10.1051/0004-6361/201935828.
- C. E. Kester, A. Bernui, and W. S. Hipólito-Ricaldi. Probing the statistical isotropy of the universe with Planck data of the cosmic microwave background. *A&A*, 683:A176, Mar. 2024. doi: 10.1051/0004-6361/202348160.
- T. M. Koshut, W. S. Paciesas, C. Kouveliotou, J. van Paradijs, G. N. Pendleton, G. J. Fishman, and C. A. Meegan. Systematic Effects on Duration Measurements of Gamma-Ray Bursts. *ApJ*, 463: 570, June 1996. doi: 10.1086/177272.
- C. Kouveliotou, C. A. Meegan, G. J. Fishman, N. P. Bhat, M. S. Briggs, T. M. Koshut, W. S. Paciesas, and G. N. Pendleton. Identification of Two Classes of Gamma-Ray Bursts. *ApJ*, 413: L101, Aug. 1993. doi: 10.1086/186969.
- C. Krishnan, R. Mohayaee, E. Ó. Colgáin, M. M. Sheikh-Jabbari, and L. Yin. Hints of FLRW breakdown from supernovae. *PRD*, 105(6):063514, Mar. 2022. doi: 10.1103/PhysRevD.105.063514.
- S. D. Landy and A. S. Szalay. Bias and Variance of Angular Correlation Functions. *ApJ*, 412:64, July 1993. doi: 10.1086/172900.
- M.-H. Li and H.-N. Lin. Testing the homogeneity of the Universe using gamma-ray bursts. *Astron. Astrophys.*, 582:A111, 2015. doi: 10.1051/0004-6361/201525736.
- M. Lopes, A. Bernui, C. Franco, and F. Avila. Bulk Flow Motion Detection in the Local Universe with Pantheon+ Type Ia Supernovae. *ApJ*, 967(1):47, May 2024. doi: 10.3847/1538-4357/ad3735.
- O. Luongo, M. Muccino, E. Ó. Colgáin, M. M. Sheikh-Jabbari, and L. Yin. Larger H_0 values in the CMB dipole direction. *PRD*, 105(10):103510, May 2022. doi: 10.1103/PhysRevD.105.103510.
- M. Magliocchetti, G. Ghirlanda, and A. Celotti. Evidence for anisotropy in the distribution of short - lived gamma-ray bursts. *MNRAS*, 343:255, 2003. doi: 10.1046/j.1365-8711.2003.06657.x.
- C. Meegan, G. Lichti, P. N. Bhat, E. Bissaldi, M. S. Briggs, V. Connaughton, R. Diehl, G. Fishman, J. Greiner, A. S. Hoover, A. J. van der Horst, A. von Kienlin, R. M. Kippen, C. Kouveliotou, S. McBreen, W. S. Paciesas, R. Preece, H. Steinle, M. S. Wallace, R. B. Wilson, and C. Wilson-Hodge. The Fermi Gamma-ray Burst Monitor. *ApJ*, 702(1):791–804, Sept. 2009. doi: 10.1088/0004-637X/702/1/791.
- C. A. Meegan, G. J. Fishman, R. B. Wilson, W. S. Paciesas, G. N. Pendleton, J. M. Horack, M. N. Brock, and C. Kouveliotou. Spatial distribution of γ -ray bursts observed by BATSE. *Nat*, 355 (6356):143–145, Jan. 1992. doi: 10.1038/355143a0.

- N. Mehta and S. Iyyani. Exploring Gamma-Ray Burst Diversity: Clustering analysis of emission characteristics of Fermi and BATSE detected GRBs. *arXiv e-prints*, art. arXiv:2402.15260, Feb. 2024. doi: 10.48550/arXiv.2402.15260.
- V. Mittal, O. T. Oayda, and G. F. Lewis. The cosmic dipole in the Quiaa sample of quasars: a Bayesian analysis. *MNRAS*, 527(3):8497–8510, Jan. 2024. doi: 10.1093/mnras/stad3706.
- W. S. Paciesas, C. A. Meegan, G. N. Pendleton, M. S. Briggs, C. Kouveliotou, T. M. Koshut, J. P. Lestrade, M. L. McCollough, J. J. Brainerd, J. Hakkila, W. Henze, R. D. Preece, V. Connaughton, R. M. Kippen, R. S. Mallozzi, G. J. Fishman, G. A. Richardson, and M. Sahi. The Fourth BATSE Gamma-Ray Burst Catalog (Revised). *ApJs*, 122(2):465–495, June 1999a. doi: 10.1086/313224.
- W. S. Paciesas, C. A. Meegan, G. N. Pendleton, M. S. Briggs, C. Kouveliotou, T. M. Koshut, J. P. Lestrade, M. L. McCollough, J. J. Brainerd, J. Hakkila, W. Henze, R. D. Preece, V. Connaughton, R. M. Kippen, R. S. Mallozzi, G. J. Fishman, G. A. Richardson, and M. Sahi. The Fourth BATSE Gamma-Ray Burst Catalog (Revised). *ApJs*, 122(2):465–495, June 1999b. doi: 10.1086/313224.
- T. S. Pereira, C. Pitrou, and J.-P. Uzan. Theory of cosmological perturbations in an anisotropic universe. *JCAP*, 09(9):006, Sept. 2007. doi: 10.1088/1475-7516/2007/09/006.
- R. D. Preece, M. S. Briggs, R. S. Mallozzi, G. N. Pendleton, W. S. Paciesas, and D. L. Band. The BATSE Gamma-Ray Burst Spectral Catalog. I. High Time Resolution Spectroscopy of Bright Bursts Using High Energy Resolution Data. *ApJs*, 126(1):19–36, Jan. 2000. doi: 10.1086/313289.
- J. Ripa and A. Shafieloo. Testing the Isotropic Universe Using the Gamma-Ray Burst Data of Fermi/GBM. *Astrophys. J.*, 851(1):15, 2017. doi: 10.3847/1538-4357/aa9708.
- L. Salmon, L. Hanlon, and A. Martin-Carrillo. Two Dimensional Clustering of Swift/BAT and Fermi/GBM Gamma-ray Bursts. *Galaxies*, 10(4):77, June 2022. doi: 10.3390/galaxies10040077.
- A. K. Singal. Large disparity in cosmic reference frames determined from the sky distributions of radio sources and the microwave background radiation. *PRD*, 100(6):063501, Sept. 2019. doi: 10.1103/PhysRevD.100.063501.
- F. Sorrenti, R. Durrer, and M. Kunz. A local infall from a cosmographic analysis of Pantheon+. *arXiv e-prints*, art. arXiv:2407.07002, July 2024a. doi: 10.48550/arXiv.2407.07002.
- F. Sorrenti, R. Durrer, and M. Kunz. The low multipoles in the Pantheon+SH0ES data. *arXiv e-prints*, art. arXiv:2403.17741, Mar. 2024b. doi: 10.48550/arXiv.2403.17741.
- M. Tarnopolski. Testing the anisotropy in the angular distribution of *Fermi*/GBM gamma-ray bursts. *Mon. Not. Roy. Astron. Soc.*, 472(4):4819–4831, 2017. doi: 10.1093/mnras/stx2356.
- P. Tiwari and P. Jain. Evidence of isotropy on large distance scales from polarizations of radio sources. *Astron. Astrophys.*, 622:A113, 2019. doi: 10.1051/0004-6361/201834192.
- T. N. Ukwatta and P. R. Wozniak. Investigation of Redshift- and Duration-Dependent Clustering of Gamma-ray Bursts. *Mon. Not. Roy. Astron. Soc.*, 455(1):703–711, 2016. doi: 10.1093/mnras/stv2350.
- R. Vavrek, L. G. Balazs, A. Meszaros, I. Horvath, and Z. Bagoly. Testing the Randomness in the Sky-Distribution of Gamma-Ray Bursts. *Mon. Not. Roy. Astron. Soc.*, 391:1741, 2008. doi: 10.1111/j.1365-2966.2008.13635.x.

- A. von Kienlin, C. A. Meegan, W. S. Paciesas, P. N. Bhat, E. Bissaldi, M. S. Briggs, E. Burns, W. H. Cleveland, M. H. Gibby, M. M. Giles, A. Goldstein, R. Hamburg, C. M. Hui, D. Kocevski, B. Mailyan, C. Malacaria, S. Poolakkil, R. D. Preece, O. J. Roberts, P. Veres, and C. A. Wilson-Hodge. The Fourth Fermi-GBM Gamma-Ray Burst Catalog: A Decade of Data. *ApJ*, 893(1):46, Apr. 2020. doi: 10.3847/1538-4357/ab7a18.
- J. Řípa and A. Shafieloo. Update on Testing the Isotropy of the Properties of Gamma-Ray Bursts. *Mon. Not. Roy. Astron. Soc.*, 486(3):3027–3040, 2019. doi: 10.1093/mnras/stz921.
- Z. Zhai and W. J. Percival. Sample variance for supernovae distance measurements and the Hubble tension. *PRD*, 106(10):103527, Nov. 2022. doi: 10.1103/PhysRevD.106.103527.